ECE 233 - Spring 2020

Wireless Communications System Design, Modeling, and Implementation

Subsampling Architecture for Ultra-Wideband (UWB)

By: Swapnil Sayan Saha and Vivek Jain

UID: 605353215 and 805418739

Date of Submission: 10th May 2020

Abstract

The wide bandwidth of ultra-wideband (UWB) radios has induced interest for indoor high-precision ranging, low-data-rate and high-speed communications and surveillance applications. With the advent of embedded systems, UWB systems covet a low-complexity, low-power and low-cost solution. In this project, we explore the performance of a low-complexity subsampling architecture for 3.1-10.6 GHz UWB systems. The system subsamples the passband impulses at twice the signal bandwidth using a high-speed, low-resolution and low-power CMOS analog-to-digital converter (ADC) and performs analytic matched filtering in the digital and complex domain to resolve timing offset sensitivity and extract granular timing information. Specifically, we study the signal-to-noise ratio (SNR) and bit error rate (BER) of the system under varying timing offsets with IEEE CM-1 channel model. We observe that an increase in timing offset results in a slight but linear decrease of SNR, which is ubiquitous for high-resolution timing information extraction. Additionally, we observe that an increase delay offset causes the BER to increase but only slightly, with the difference more pronounced at high SNR values, proving that the architecture is capable of handling varying timing offsets without loss of information.

1 System Model

The Federal Communications Commission (FCC) defines UWB systems as wireless transmission schemes occupying a fractional bandwidth of 0.2 or more or an absolute bandwidth of 500 MHz or more [1]. The wide bandwidth and impulse signaling scheme of UWB radios support high-data-rate communication in additive white Gaussian noise (AWGN) environments without requiring high-power transmitters, sophisticated error correction mechanisms or high order modulation [1]. Furthermore, increasing the bandwidth also results in fine delay resolution in multipath environments (such as residential line-of-sight (LOS) as described by IEEE CM-1), allowing for applications such as precision localization, indoor communication systems, medical imaging, surveillance and vehicular usage [1][2]. There are three FCC-approved UWB frequency bands: 0-960 MHz, 3.1-10.6 GHz and 22-29 GHz, of which 3.1-10.6 GHz is unlicensed for indoor usage without user limitations [2][3], also called IEEE 802.15.4 [4]. Characteristics of 3.1-10.6 GHz band include short-range personal area networking (PAN) capabilities (4-10 meters), data rates ranging from 110 to 200 Mbps, channel bandwidth of 500 MHz to 7.5 GHz, 1-15 RF channels, BPSK/QPSK modulation scheme, multiband spreading, maximum RF power of -41.3 dbm/MHz and maximum power consumption of 2-3 BT [5].

The advent of Internet-of-Things (IoT) has resulted in embedded systems that are low-cost, low-power, reduced footprint and high-performance characteristics [6]. As a result, UWB systems intended for PAN sensor networks and low-data-rate communication require a low-cost, low-power and reduced complexity radio architecture [3] to complement the sensing and actuating components. Traditional approaches such as multiband-OFDM, Rake reception and generic transmitted reference (TR) schemes suffer from increased receiver complexity, implementation cost, large power footprint and poor SNR [3][4]. Keeping the challenges in mind, we study the performance of a simple UWB receiver introduced in [3] utilizing a subsampling analog frontend and operating in the digital and complex baseband domain on analytic signals without sacrificing delay resolution. In particular, we evaluate how the receiver architecture responds to timing sensitivity issue (innate in subsampling systems) with the SNR and BER as performance metrics.

For the system model, we consider a simplified version of the impulse radio UWB TR signal introduced in [4], omitting the terms relevant to reference signal and time hopping sequence (underlined in equation (1)) and keeping only the data signal.

$$s_{TX}(t) = \sqrt{\frac{E_s}{2N_f}} \sum_{j=-\infty}^{\infty} d_j [\underline{w_{tx}(t - jT_f - c_j T_c)} + b_{\lfloor j/N_f \rfloor} w_{tx}(t - jT_f - \underline{c_j} T_c - \underline{T_d})] \tag{1}$$

$$\Rightarrow s_{TX}(t) \simeq \sqrt{\frac{E_s}{2N_f}} \sum_{j=-\infty}^{\infty} d_j b_{\lfloor j/N_f \rfloor} w_{tx}(t - jT_f)] \tag{2}$$

where,

- E_s denotes the signal energy per transmitted symbol, assumed to be unit energy.
- N_f denotes the number of frames per symbol, assumed to be 10 as per [4]. d_j represents a pseudo-random (PN) sequence of +1 and -1 with mean 0, useful for pulse shaping.
- $b_{\lfloor j/N_f \rfloor} \in \{-1, +1\}$ is the BPSK modulated information signal.
- w_{tx} is the unit energy transmit waveform, which we considered as Gaussian modulated RF impulse of central frequency, $f_c = 3.5$ GHz and bandwidth, $B = 1$ GHz.
- T_f is the frame duration, given as: $T_f = T_s/N_f$, where T_s is the symbol duration and given as $T_s = 1/B$.

Given the constraints on the size of binary information signal, j is constrained within $[-N_f^2, N_f^2]$.

For the channel, we assume IEEE CM-1 channel model, referring to residential LOS conditions [7][8]. The model parameters are populated in Table 1:

Table 1: Model Parameters for IEEE CM-1 / Residential LOS [7]

Parameter	**Value**
Pathloss parameters	
PL_0 (dB), path loss at 1m distance	43.9
n, pathloss exponent	1.79
σ_{S} (dB), shadowing standard deviation	2.22
A_{ant} (dB), antenna loss	3
κ, frequency dependence of path loss	1.12±0.12
Power delay profile parameters	
$\hat{L}$, mean number of clusters	3
$\Lambda(\text{ns}^{-1})$, inter-cluster arrival rate	0.047
λ_1, λ_2 (ns^{-1}), β, ray arrival rates from mixed Poisson model	1.54, 0.15, 0.095
Γ (ns), inter-cluster decay constant	22.61
k_γ, intra-cluster decay time constant parameter	0
γ_0 (ns), intra-cluster decay time constant parameter	12.53
σ_{cluster} (dB), cluster shadowing variance	2.75
Small-scale fading parameters	
m_0 (dB), Nakagami m factor mean	0.67
k_m, Nakagami m factor mean	0
$\widehat{m_0}$ (dB), Nakagami m factor variance	0.28
$\widetilde{m_0}$, Nakagami m factor for strong components	-
$\widehat{k_m}$, Nakagami m factor variance	0

We assume that the environment has the Saleh-Valenzuela (S-V) shape and the impulse response of the IEEE CM-1 channel is generated as follows [7]:

- Calculate the number of clusters L (rays arrive in clusters in SV model) as Poisson distributed random variable:

$$pdf_L(L) = \frac{(\bar{L})^L e^{(-\bar{L})}}{L!} \tag{3}$$

For each cluster l in L:

- generate cluster decay time γ_t and total cluster power Ω_t as follows:

$$\gamma_l = k_\gamma T_l + \gamma_0 \tag{4}$$

$$10\log(\Omega_t) = 10\log(e^{\frac{-T_l}{\Gamma}}) + \mathcal{N}(0, \sigma^2_{\text{cluster}}) \tag{5}$$

T_l (cluster arrival time) is initially 0 and updated over each pass in the clusters.

For each component (or ray) k in l, as long as first ray arrival time $\tau_{k,l}$ (initially 0) is less than $10\gamma_l$:

- Compute mean power delay profile of kth component as follows:

$$E\{|a_{k,l}|^2\} = \frac{\Omega_t e^{\frac{\tau_{k,l}}{\gamma_l}}}{\gamma_l[(1-\beta)\lambda_1 + \beta\lambda_2 + 1]} \tag{6}$$

- If $\beta > \mathcal{U}(0,1)$, update $\tau_{k,l}$ as per equation (7), else use equation (8).

$$\tau_{k,l} = \tau_{k,l} + [\mathcal{N}(0, \frac{1}{\sqrt{2\lambda_1}})]^2_1 + [\mathcal{N}(0, \frac{1}{\sqrt{2\lambda_1}})]^2_2 \tag{7}$$

$$\tau_{k,l} = \tau_{k,l} + [\mathcal{N}(0, \frac{1}{\sqrt{2\lambda_2}})]^2_1 + [\mathcal{N}(0, \frac{1}{\sqrt{2\lambda_2}})]^2_2 \tag{8}$$

- Set m-factor for each first component k to $\widetilde{m_0}$.

- Compute mean and variance of m-factor for all other components as follows:

$$\mu_m(T_l, \tau_{k,l}) = m_0 - k_m(T_l + \tau_{k,l}) \tag{9}$$

$$\sigma_m(T_l, \tau_{k,l}) = \widehat{m_0} - \widehat{k_m}(T_l + \tau_{k,l}) \tag{10}$$

- Generate log-normal distributed Nakagami amplitude realization as follows:

$$ln(m_{l,k}) \sim \mathcal{N}(\mu_m(T_l, \tau_{k,l}), \sigma_m(T_l, \tau_{k,l})) \tag{11}$$

For each cluster l in L:

- Update T_l as:

$$T_l = T_l + [\mathcal{N}(0, \frac{1}{\sqrt{2\Lambda}})]^2_1 + [\mathcal{N}(0, \frac{1}{\sqrt{2\Lambda}})]^2_2 \tag{12}$$

For each path q in all clusters $l \in L$ (q is the total number of rays or components):

- Compute continuous time impulse response from Gamma distribution as follows:

$$h_q \sim \sqrt{\Gamma(m_q, \frac{h_q}{\sigma_q})} \tag{13}$$

- Change continuous time impulse response to complex baseband as follows:

$$h_{q,\text{complex}} = h_q e^{j \cdot \mathcal{U}(0,2\pi)} \tag{14}$$

- Change continuous time complex impulse response to discrete time impulse response via re-sampling (using symbol duration T_s in the pipeline)

- Add frequency dependency and normalize channel energy as follows:

$$h = \frac{\mathcal{F}^{-1}(\mathcal{F}(h_{\text{complex}} \cdot f))}{\sqrt{h^T h}}, f \in [\frac{fc - B}{2f_d}, \frac{fc + B}{2f_d}]^{-2\kappa} \tag{15}$$

Code for IEEE CM-1 channel model and further details is available in [7]. Fig. 1 shows sample UWB signal and channel impulse response generated from one Monte Carlo trial.

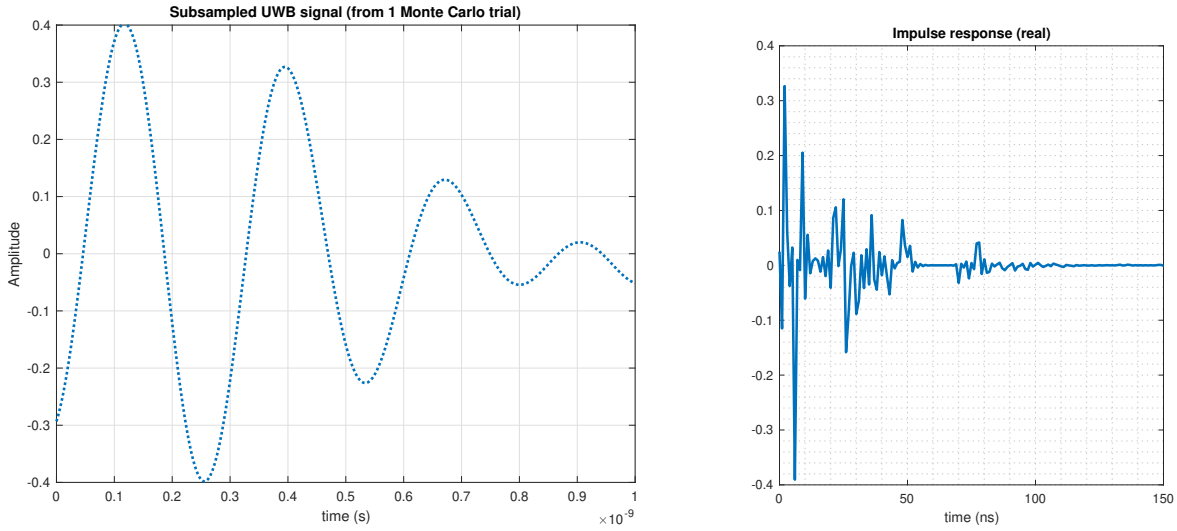

Figure 1: (Left): Subsampled UWB signal shape (generated from one Monte Carlo trial) (Right): Generated sample IEEE CM-1 channel impulse response (real).

2 Receiver Architecture and Techniques

Fig. 2 shows overview of the subsampling receiver architecture along with datapath of proposed complex digital baseband [3].

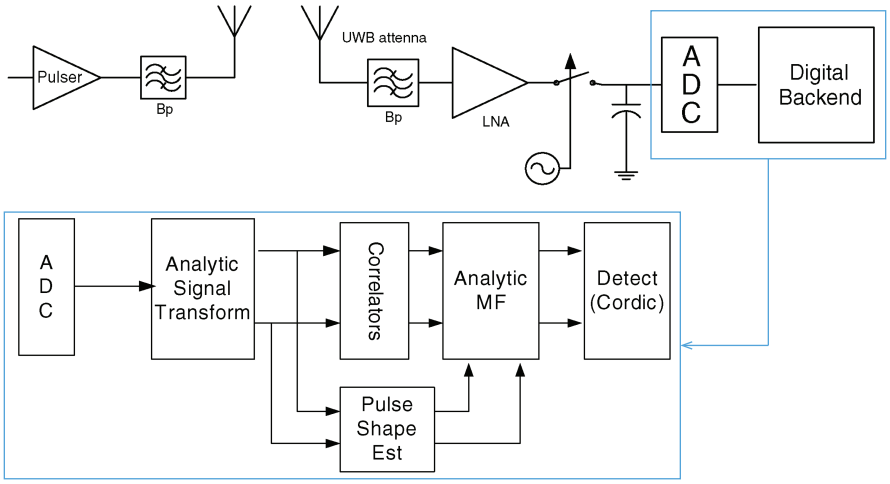

Figure 2: Receiver architecture and digital baseband datapath (Credit: [3])

The subsampling ADC samples the signal at twice the bandwidth instead of maximum signal frequency in order to minimize signal aliasing via a low undersampling ratio. The subsampling architecture maintains a high signal bandwidth up to sampling circuitry and the low undersampling ratio decreases the amount of extra thermal noise folding into the signal spectrum. Since SNR of UWB signals is relatively low due to power regulation and large inband noise power, the subsampling frontend requires only a low-resolution (4-6 bit) ADC. Since quantization noise of ADC dominates thermal noise from the sampling circuit, overall system performance degradation due to the sampling circuit is negligible. Furthermore, UWB requires a low Q bandpass filter, allowing the subsampling frontend to be packaged in low-power CMOS footprint, reducing discrete component count and power consumption [3].

A key problem with the subsampling architecture is the sub-optimal signal detection due to timing mismatch between energy detector (matched filter) and sampled signal, more pronounced than Nyquist sampling architecture. An analytic signaling approach in the digital and complex baseband domain can help mitigate the problem. The analytic signal transform is a 21-point FIR Hilbert transform that projects the signal to an orthogonal space. Compared to differentiator (ideal), the Hilbert transformer is a wideband phase shifter and does not suffer from non-flat gain response (which can cause aliasing and noise amplification), resulting in negligible SNR degradation compared to differentiator analytic transform [3]. The Hilbert transform is given as follows:

$$\mathcal{H}[s(t)] = \frac{1}{\pi t} * s(t) \overset{\mathcal{F}.\mathcal{T}.}{\Longleftrightarrow} -j \cdot sign(\omega) \cdot S(\omega) \tag{16}$$

The output of the Hilbert transform is expressed as:

$$\tilde{s}(t) = \mathcal{H}[s(t)] = s_r(t) + j s_i(t) \tag{17}$$

To incorporate the channel model, the channel impulse response $h_{\text{CM-1}}$ needs to be convolved with the $s(t)$, which is only required for BER analysis.

The correlators are are used for de-spreading modulated code and increase processing gain. The pulse-shape estimator uses maximum likelihood (running average) over the PN sequence (within coherence time) for optimal detection. The detector decodes data or timing information after intersymbol interference (ISI) is mitigated with complex equalizer. The main component in the digital backend is the analytic matched filter (MF), which acts as an energy detector in the presence of AWGN [3]. The impulse response of the MF is given by:

$$\tilde{h}(t) = h_r(t) + jh_i(t) = s_r^*(T-t) + js_i^*(T-t) \tag{18}$$

$T = b - a$ is the time where UWB pulse exists without ISI. The output of the MF given the input signal $y_r(t) + jy_i(t)$ is given by:

$$m_r + jm_i =< y_r, h_r > + < y_i, h_i > +j(- < y_r, h_i > + < y_i, h_r >) \tag{19}$$

The operator $< x, y >$ is defined as:

$$< x, y >= \int_a^b x(t) \cdot y(T-t)dt \tag{20}$$

The input signal $y(t)$ after applying delay offset T_0 and adding AWGN $(n_r + jn_i)$ is given as:

$$y(t) = \mathcal{F}^{-1}[\mathcal{F}[\tilde{s}(t) \cdot e^{jk(2\pi/T_s)T_0}]] + (n_r + jn_i) \tag{21}$$

- For noiseless case with no timing offset, input signal is same as $\tilde{s}(t)$. All the signal energy will thus concentrate on the real part of the analytic MF and the output of the matched filter is as follows:
$$m_r + jm_i = E_r + E_i = \int_a^b s_r^2(t)dt + \int_a^b s_t^2(t)dt = 2E_s \tag{22}$$
- For noiseless case with timing offset, a phase shift is introduced at the output of the Hilbert transform, given by $e^{\pm jk(2\pi/T_s)T_0}$. This will cause a redistribution of signal energy in the real and complex part of the MF and the outputs will be given as:
$$m_r + jm_i = 2E_s \cos(\frac{2k\pi T_0}{T_s}) - j(2E_s \sin(\frac{2k\pi T_0}{T_s})) \tag{23}$$
The output of matched filter will conserve the entire signal energy.
- For noisy input with timing offset, the output of the MF is given as:
$$m_r + jm_i = 2E_s \cos(\frac{2k\pi T_0}{T_s}) + n_{mr} - j(2E_s \sin(\frac{2k\pi T_0}{T_s}) + n_{mi}) \tag{24}$$
$$n_{mr} =< n_r, h_r > + < n_i, h_i > \sim \mathcal{N}(0, \sigma_n^2) \tag{25}$$
$$n_{mi} = - < n_r, h_i > + < n_i, h_r > \sim \mathcal{N}(0, \sigma_n^2) \tag{26}$$
n_r, n_i refer to real and imaginary parts of AWGN. The conservation of entire signal energy causes noise to be conserved at the output of the MF, causing degradation in performance. The SNR at the output of the MF given by:
$$\text{SNR}_R(\frac{2E_s}{\sigma_n} = \alpha) = \frac{(E(R)|_{\frac{2E_s}{\sigma_n}=\alpha} - E(R)|_{\frac{2E_s}{\sigma_n}=0})^2}{Var(R)|_{\frac{2E_s}{\sigma_n}=\alpha}} \tag{27}$$

R is the magnitude of the MF given as:

$$R = \sqrt{m_r^2 + m_i^2} \tag{28}$$

From equation (27), we can similarly derive the output of the real part of the matched filter, given as:

$$SNR_{m_r}(\frac{2E_s}{\sigma_n} = \alpha) = \frac{(E(m_r)|_{\frac{2E_s}{\sigma_n}=\alpha} - E(m_r)|_{\frac{2E_s}{\sigma_n}=0})^2}{Var(m_r)|_{\frac{2E_s}{\sigma_n}=\alpha}} = \frac{\alpha^2}{4} \cdot \cos^2(\frac{2k\pi T_0}{Ts}) \tag{29}$$

Equation (29) hints that the output of ideal filter (which projects signal onto real plane) will have SNR dips as timing offset alters. However, since analytic MF takes both real and imaginary components, performance degradation is mitigated. As timing offset increases, we should observe only a slight decrease in SNR at the output of analytic MF, with SNR nulls in real and imaginary components as timing offset increases as shown by equation (29). For our analysis, we consider noisy input with timing offset from 0 to T_s. Since SNR at the output of matched filter decreases as delay offset increases, we would also expect the BER to increase as timing offset increases, with the effects more pronounced at higher SNR.

MATLAB Implementation and Further Assumptions

For SNR-delay offset analysis, the main challenge was to implement the analytic MF in MATLAB. In order to do so, we first generated the subsampled wideband signal. We created a PN sequence of +1 and -1 and ensured the mean is close to 0 and used a single symbol, i.e. 10 bits (N_f=10), with the pulse being a Gaussian modulated RF pulse with f_c = 3.5 GHz and B = 1 GHz. Note that for analysis of SNR-delay offset, one does not require the channel model as per [3]. For ease of simulation, we assume very high frequency sampling at over 10 GHz for discretizing our subsampled signal. After modulation, we convert the UWB pulse to a unit energy signal and then pass it through a Hilbert transformer implemented using `hilbert()` function in MATLAB. This generated the desired analytic signal. In order to do the analysis of timing offset on MF output SNR, the timing offset is simulated as a phase shift in Fourier (frequency) domain. This is done by taking a FFT of the signal and then phase shifting the signal with appropriate frequency scaling followed by scaled IFFT to get the time domain signal again. The analytic MF is implemented as an inner product operator. The real signal is composed of inner product of real parts of both the signal and inner product of imaginary parts of both signals as per equation (19). The quadrature signal, on the other hand is composed of inner product of real or I phased signal and complex or Q phased matched pulse and vice versa as per equation (19). In order to understand the characteristic of noise in limited number of Monte-Carlo trials without blowing the simulator, we take the power of noise as variance directly in order to compute the SNR as per equation (27) and the matched signal is given by vector sum of real part and imaginary parts. The SNR of the system is assumed to be at 20 dB and the system is simulated for 1000 Monte Carlo trials.

For the second part, the aim was to study the effect of timing offset on BER for IEEE CM-1. In order to do this, we first assume that there is only one user, which eliminates the need for PN sequence and hence the receiver architecture simplifies to only MF and detector. We also assume that the system is locked on to LoS channel path (single channel tap), which is a common assumption in UWB system simulations [9][10]. The SNR of the system is variable from 0 to 20 dB and noise is generated accordingly. In order to simulate the timing offset, we again use FFT and IFFT to implement phase shift. Assuming the channel is known (i.e. channel estimation has been done using TH sequence / pilots introduced in [4]), we latch on to the LoS component with highest gain. This is then matched with the Gaussian pulse at that instance and the detection depends on the sign of the matched signal. A positive value would mean +1 and a negative would mean -1 in the BPSK constellation. We implement the system for 5000 Monte Carlo trials and 3 different timing offsets.

3 Results and Discussion

Fig 3. shows the SNR plot for real, imaginary and magnitude parts of the detected signal at the output of the MF for different timing offsets varying from 0 to $1T_s$ for a system operating at 20 dB.

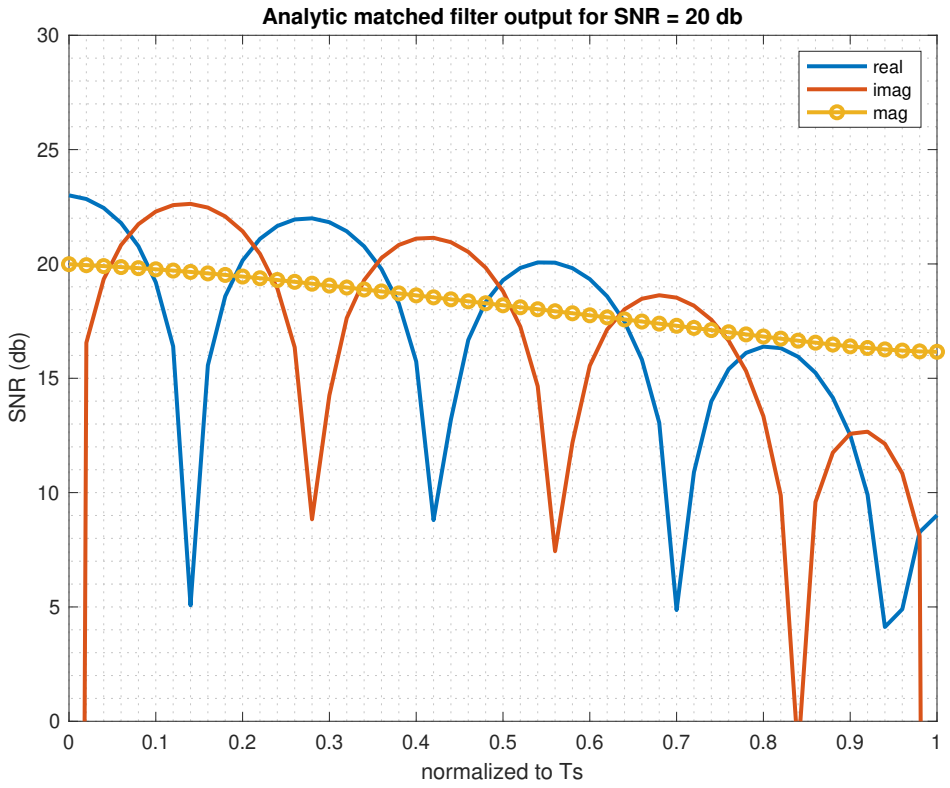

Figure 3: SNR at the output of analytic MF after 1000 Monte Carlo trials.

From Fig. 3, we observe that the matched filter gives the perfect system SNR (input and output match) for no timing offset. This shows the system is less affected by noise and rather timing offset

plays a crucial role, in line with equation (24). Furthermore, we can observe that in case of ideal system (no timing offset) there is negligible power in the complex part, which agrees with equation (22). However, as timing offset increases, we see SNR nulls/dips in the real and complex parts as predicted by equation (29). This justifies the use of matched filter over ideal filters (real-valued filters), as the original signal content is retrieved regardless of whether signal energy is distributed in the real or complex part as per equation (29). As timing offset increases, we observe oscillation in real and imaginary components of SNRs (while the magnitude decreases linearly slightly), which occurs because the signal phases are no longer orthogonal. Thus, there is a correlation between the I phase and Q phase causing the mismatch. This happens because the timing delay acts like a phase shift in frequency domain. The plot obtained mimics the plot obtained in [3], Fig. 8, which proves that our plot is correct.

Fig 4. shows the BER vs SNR plot at the output of the MF for different three timing offsets (0, $0.5T_s$ and T_s), with system SNR varying from 0 to 20 dB.

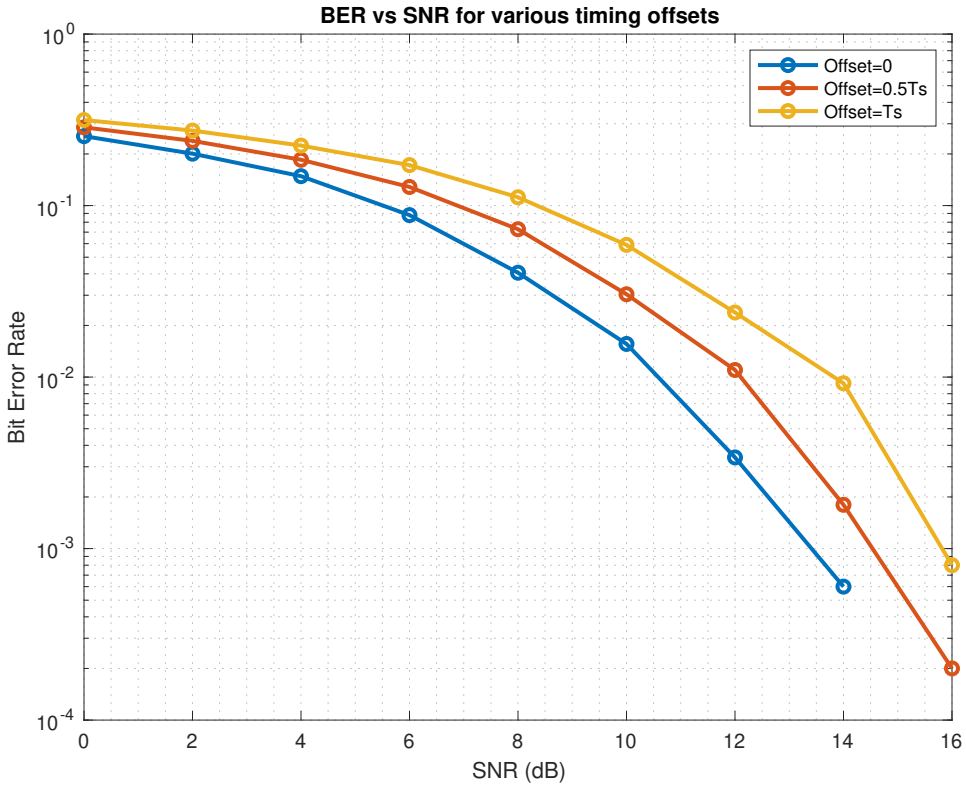

Figure 4: BER vs SNR plot for different timing offsets after 5000 Monte Carlo trials.

From Fig. 4, we observe that as delay offset increases, we get a degraded performance in BER. This is in line with our observations in part 1 where we saw the SNR of the system decreases linearly for increase in timing offset. Additionally, due to the limited number of Monte-Carlo trials, we get

negligible bit errors if SNR exceeds 16 dB. Note that the BER spacing is more pronounced when the SNR of the system is extremely high, however, this is rarely the case for ideal UWB systems. Fow low SNRs, we see that the analytic MF and detector performs almost similarly for all timing offsets. This is expected because analytic MF is supposed to be less sensitive to timing offsets [3], with only linear/predictable dependence of output SNR on timing offsets.

4 Conclusion

In this project, we have implemented and studied the performance of a subsampling architecture for UWB radio that is intended to reduce power consumption, cost, implementation complexity and component footprint. We observe that the use of analytic MF mitigates timing sensitivity issues, with only a slight linear and predictable decrease in the SNR of the system with increase in timing offset. We also observe that the BER of the system degrades only slightly when timing offset is introduced, with the system performance being similar for varying timing offsets at low SNR. As a result, the architecture is suitable for granular timing extraction and information exchange applications.

References

[1] S. Roy, J. R. Foerster, V. S. Somayazulu and D. G. Leeper, *Ultrawideband radio design: the promise of high-speed, short-range wireless connectivity*, in Proceedings of the IEEE, vol. 92, no. 2, pp. 295-311, Feb. 2004.

[2] Scholtz, Robert A., Davida M. Pozar, and Won Namgoong. *Ultra-wideband radio.* EURASIP Journal on Advances in Signal Processing 2005.3 (2005): 758540.

[3] S. M. Chen and R. W. Brodersen, *A Subsampling Radio Architecture for Ultrawideband Communications*, in IEEE Transactions on Signal Processing, vol. 55, no. 10, pp. 5018-5031. Oct. 2007.

[4] F. Tufvesson, S. Gezici and A. F. Molisch, *Ultra-Wideband Communications using Hybrid Matched Filter Correlation Receivers*, in IEEE Transactions on Wireless Communications, vol. 5, no. 11, pp. 3119-3129, November 2006,

[5] D. Porcino and W. Hirt, *Ultra-wideband radio technology: potential and challenges ahead*, in IEEE Communications Magazine, vol. 41, no. 7, pp. 66-74, July 2003.

[6] A. S. Vale-Cardoso, M. Geny Moreira, C. H. N. Martins and M. C. R. Leles, "IoT Embedded Computing Systems Performance Assessment: a Simple Method," 2019 IEEE 10th Annual Information Technology, Electronics and Mobile Communication Conference (IEMCON), Vancouver, BC, Canada, 2019, pp. 0071-0075.

[7] Molisch, Andreas F., et al. *IEEE 802.15. 4a Channel Model-Final Report.* IEEE P802 15.04 (2004): 0662.

[8] A. F. Molisch, J. R. Foerster and M. Pendergrass, *Channel models for ultrawideband personal area networks*, in IEEE Wireless Communications, vol. 10, no. 6, pp. 14-21, Dec. 2003.

[9] Falsi, Chiara, et al. *Time of arrival estimation for UWB localizers in realistic environments.* EURASIP Journal on Advances in Signal Processing 2006.1 (2006): 032082.

[10] Dardari, Davide, Chia-Chin Chong, and Moe Win. *Threshold-based time-of-arrival estimators in UWB dense multipath channels.* IEEE Transactions on Communications 56.8 (2008): 1366-1378.